

Simulation Model Update and Optimized Control Design of a Sub-Scale Flybarless Helicopter

Jeffrey Walker
Bihrl Applied Research
Hampton, VA, USA

Mark B. Tischler
Tischler Aeronautics
Sunnyvale, CA, USA

ABSTRACT

This paper demonstrates simulation model updates using black-box filters and the application of Froude scaled ADS-33 specifications to design an inner- and outer-loop control system for a sub-scale flybarless helicopter. The black-box filters provide a simple and effective update to the vehicle plant resulting in accurate translation of design to flight. Design specifications for manned rotorcraft specified by ADS-33 are Froude scaled and applied as design minimums with adjustments made to accommodate limiting vehicle dynamics. The control system is optimized using CONDUIT[®] and design margin optimization is used to maximize the vehicle performance. Flight testing is conducted to validate the control laws using system identification and the vehicle performance is demonstrated using scaled Mission Task Elements.

INTRODUCTION

Small Unmanned Aircraft Systems (UAS) provide new opportunities that benefit civilian, commercial, and military users with a wide range of applications. In recent years the Federal Aviation Administration (FAA) has introduced type certification for UAS using a Durability and Reliability process which is intended to demonstrate that the UAS is *reliable, controllable, and safe* based on flight test demonstration over the expected flight envelope (Ref. 1). The Durability and Reliability process does not impose any low-level flight control requirements and instead focuses on the complete end-to-end system using a risk-based approach. Small UAS often use high level flight modes common to off-the-shelf autopilot packages such as PX4 (Ref. 2) and ArduCopter (Ref. 3) which often rely on empirical gain tuning or in-flight auto-tuning as a low-cost solution to get a vehicle airborne. However, the success of the UAS is ultimately dependent on the safe and reliable operation of the underlying vehicle control system. Thus, a rigorous and methodical control design approach should be employed that uses engineering analysis and design standards to ensure safe, predictable, and reliable operation.

Model based control design provides a systematic approach to the design and analysis of the flight critical control systems and is commonly used in the development of manned aircraft. This approach requires an accurate vehicle model which can be obtained from flight tests using system identification, as described in Reference 4, or from rigorous application of first principles. For small UAS, system identification is a practical and effective solution that can produce an accurate model. Overall system deficiencies, either from poor data

quality or unmodeled dynamics, negatively impact the accuracy of model-based control design and must be corrected to ensure design model predictions are actualized in flight. In the current case model deficiencies are associated with wear and tear and associated changes in rigging during the overall project of approximately two years. The NATO AVT-296 working group compiled a comprehensive report, “Rotorcraft Flight Simulation Model Fidelity Improvement and Assessment” (Ref. 5), which covered seven methods of increasing complexity to address model deficiencies. Though the NATO report is focused on updating physics based models, these methods are equally applicable to models developed using system identification. Black-box filters, Method #2 in Reference 5, was applied to the CH-47, EC-135, and Bell 412 helicopters in Reference 6 which demonstrated the effectiveness of this relatively simple correction method.

Control system design using model-based techniques typically employs numerous specifications that impose minimums on system stability, robustness, and key handling qualities metrics. The design minimums specific to rotorcraft are established by ADS-33 and are based on extensive research and flight test experience (Ref. 7). Further, ADS-33 defines Mission Task Elements (MTEs) that specify standardized maneuvers for the evaluation of the control system performance. Recent research has focused on the application of these full-scale specifications in the design and evaluation of multirotor UAS. In Reference 8, performance based disturbance rejection was investigated for a quadrotor and was demonstrated to provide significant performance improvements over an empirically tuned controller. References 9 and 10 applied Froude scaling in the design and evaluation of a multirotor in order to meet scaled handling qualities and MTEs. This work validated the proposed application of Froude scaled ADS-33 specifications and MTEs as a framework for developing small

Presented at the Vertical Flight Society’s 78th Annual Forum & Technology Display, Ft. Worth, Texas, USA, May 10–12, 2022. Copyright © 2022 by the Vertical Flight Society. All rights reserved.

UAS control systems. Unlike multirotors, limited research has been conducted on helicopter UAS with Reference 11 being an example that investigated MTEs using Froude and Mach scaling to evaluate three dissimilar controllers in simulation.

The current effort extends the previous research of Reference 12 which identified an accurate bare-airframe model using frequency domain system identification and developed an inner-loop controller using model-based design with a limited set of stability requirements. A key distinction in the current work from the previous effort is the use of CONDUIT[®] to optimize the controllers which facilitates a multi-objective parametric optimization design (Ref. 13). This design approach allows a common set of design requirements to be used and has been demonstrated to produce similar vehicle performance irrespective of control law architecture used (Refs. 14, 15). A driving factor of the design is the appropriate selection of specifications such as disturbance rejection (Ref. 16), stability margins (Ref. 17), actuator rate limitations and Open Loop Onset Point (OLOP) (Ref. 13), and handling qualities with ADS-33 specifying a comprehensive set of handling qualities requirements for manned rotorcraft (Ref. 7). Each specification in CONDUIT[®] consists of three levels corresponding to the Cooper-Harper handling-qualities rating scale where Level-1 handling-qualities are always desired; thus, the Level 1/2 boundary represents the minimum acceptable design.

Black-box filters are first developed to provide a simulation model update to the originally identified vehicle. These input filters ensure the design model accurately predicts flight performance and flight test data demonstrates the improved model agreement. Froude scaling is then used to establish reasonable design minimums for the inner- and outer-loop controllers using ADS-33 specifications. CONDUIT[®] is used to optimize the controllers and the implications of the rotor/fuselage coupling on the Froude scaled design specifications is discussed. The performance improvements of the optimized inner-loop design are demonstrated in simulation and compared to the previous design (Ref. 12). Lastly, the controllers are validated in flight and the performance is evaluated using scaled MTEs.

PREVIOUS DEVELOPMENT

The previous research of Reference 12 applied system identification techniques to identify and model the bare-airframe vehicle dynamics of the sub-scale Blade 360CFX 3S helicopter depicted in Figure 1. This sub-scale flybarless helicopter has a main rotor diameter of 0.8121 (m) resulting in a Froude scale of $N = 20$ when using the UH-60 as the full size reference vehicle (Ref. 4). The identified model facilitated model-based control design of an Attitude Command Attitude Hold (ACAH) inner-loop controller using an Explicit Model Following (EMF) architecture.

Frequency sweep flight test data was used with CIPHER[®] to identify the model with excellent agreement up to 100 (rad/s) (Ref. 12). The hybrid formulation was used to explicitly model the coupled fuselage/rotor flapping dynamics facilitating the second-order regressive flapping mode to be accurately



Figure 1. Blade 360CFX 3S Helicopter

captured (Ref. 4). This accurate vehicle model is a prerequisite to the development of high-bandwidth flight control using model based design.

The previous ACAH control design presented in Reference 12, herein referred to as V77, was developed using Simulink[®] Control Design Toolbox. The design used a limited set of requirements emphasizing stability margins, crossover, and disturbance attenuation using tuning goals available in the Simulink[®] Control Design Toolbox. This design resulted in a suboptimal solution and required an ad-hoc approach with manual tuning to arrive at a reasonable design.

BLACK-BOX FILTERS

Method #2 of Reference 5, black-box filters, are non-physical corrections that provide additional flexibility over a simple gain and time delay (Method #1). These filters can be applied as either input or output corrections without altering the underlying baseline model (Ref. 6). Further, black-box filters can be applied to either single input, single output (SISO) or multi input, multi output (MIMO) systems. The filters can be developed using algebraic, time-domain or frequency-domain techniques (Ref. 5). In this effort the black-box filters are developed as SISO input corrections in the frequency domain.

Model Update Using Input Filters

The vehicle was subject to wear and tear and rigging changes affiliated with the flight test program which altered the vehicle bare-airframe dynamics. Black-box input filters were selected as the method to update the model as the previously identified bare-airframe model had excellent agreement with the original flight test data. Frequency sweep flight tests were conducted with the sweep injected at the effective plant input denoted by $\delta_{lat_{BL}}$ in Figure 4. The effective plant response, $G = p' / \delta_{lat}$ for the lateral axis, was constructed and the error response defined by Equation 1 was calculated in the frequency domain using the Arithmetic Utility in CIPHER[®]. Figure 2 depicts the p' / δ_{lat} error response and represents the change in the vehicle dynamics which must be updated.

$$e(s) = G_{FT}(s) / G_{design}(s) \quad (1)$$

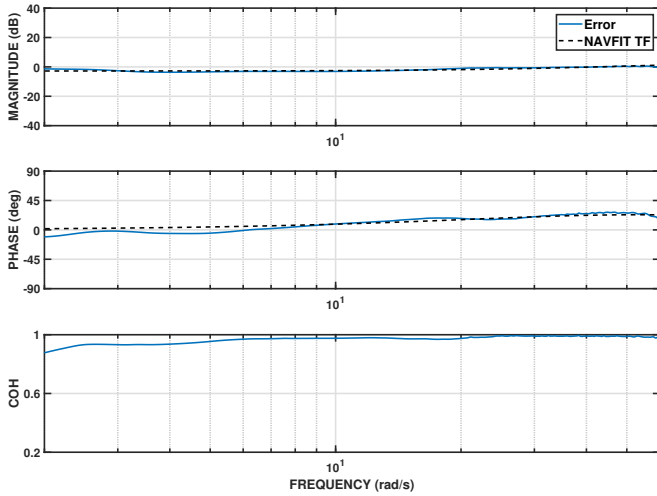


Figure 2. Lateral Error Response and Identified Input Correction

The black-box filter was identified directly from the error response using NAVFIT in CIFER® using a low-order transfer function with the generalized form of Equation 2 to avoid over-fitting. The frequency range used for identifying the filter was centered around the crossover frequency making sure to include the 180 degree phase crossing. This ensures the underlying baseline model is updated in the key frequency range of interest for control design purposes. The black dashed line in Figure 2 depicts the identified black-box filter for the lateral axis which has excellent agreement in the frequency range of 2 – 60 (rad/s).

$$\frac{s+b}{s+a}e^{-\tau s} \quad (2)$$

Filters were identified for all axes and applied to the input of the effective plant ahead of the mixer and crossfeed matrix as indicated in Figure 4. Use of input filters, in contrast to output filters, facilitates a single update that corrects the inner-loop and kinematically coupled outer-loops. Figure 3 demonstrates the improvement obtained by application of the black-box input filters where the corrected response (COR) is represented by the black dashed line and the uncorrected response (UNC) is shown in red. The quadratic cost can be used to quantitatively describe the improved model agreement where a cost of 100 denotes acceptable model agreement and 50 is excellent (Ref. 4). The corrected response has excellent agreement with a cost of 16.55, a 90% reduction from the uncorrected cost of 180.

INNER-LOOP CONTROL DESIGN

The inner-loop controller uses the same architecture of Reference 12 and provides ACAH in the lateral and longitudinal axes and Rate Command Attitude Hold (RCAH) in the directional axis. All three axes use EMF, as depicted in Figure 4 for the lateral axis. A key benefit of the EMF architecture is the

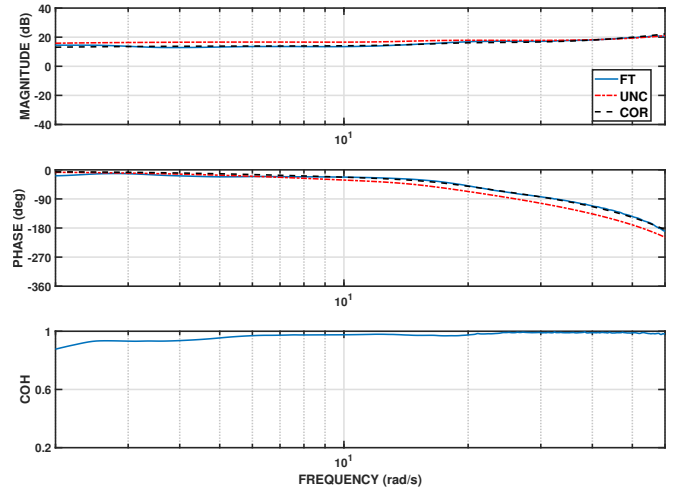


Figure 3. Lateral Corrected Response, p'/δ_{lat}

two degree of freedom design it affords. This allows the feedback response loop and command response characteristics to be designed independently (Ref. 13).

The forward path provides design freedom in the command response characteristics and consists of three key components. The command model shapes the desired response; here the lateral and longitudinal axes use a critically damped second-order response and a first-order response in the directional axis. The equivalent delay synchronizes the generated command with the measured states and helps prevent the actuators from being overdriven. The inverse plant generates feed-forward actuator inputs based on an accurate low-order equivalent system of the on-axis bare-airframe response.

The feedback path establishes the closed-loop stability and disturbance rejection characteristics. In this application a proportional-integral (PI) controller is used as depicted in Figure 5. The integrator contribution $K_{i/p}$, is constrained to 1/5 the crossover frequency which ensures the integrator is effective without degrading the phase margin (Ref. 13). Though not required in either the lateral or longitudinal axes, the directional axis uses a lead-lag filter on the output of the PI feedback to shape the response and meet stability requirements. All axes employed a low-pass filter with a break frequency of 60 (rad/s) to ensure energy dissipation at high frequencies.

Optimization Using CONDUIT®

Table 1 presents the specifications used for the inner-loop design and indicates which specifications were Froude scaled. Froude scaling is required for specifications that have dimensional units such as bandwidth (rad/s) and is not applied to non-dimensional specifications such as damping ratio and stability margins. This scaling ensures the Level 1/2 minimums, which have been developed for full-scale vehicles, are appropriate for the sub-scale helicopter. The scaled specifications of Table 1 all use the frequency scaling law $\omega \propto \sqrt{N}$. Note the minimum crossover frequency required a *reduced* Froude scale to provide a feasible solution due to the rotor/fuselage

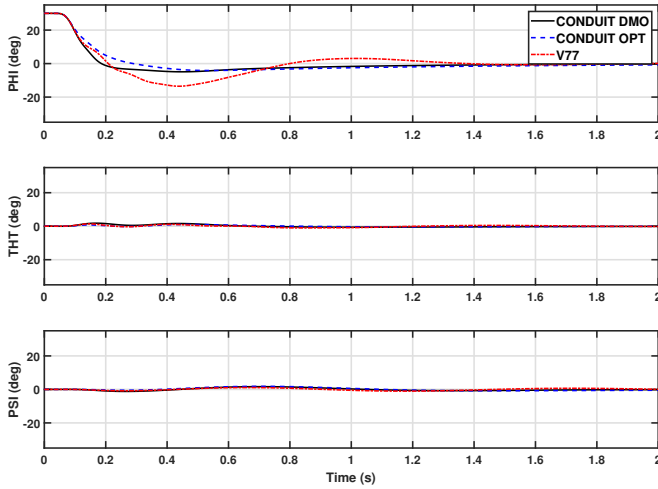


Figure 6. Disturbance Response Simulation for Roll Initial Condition Offset

with the lateral/longitudinal axes attaining a nearly $\approx 40\%$ increase. Unlike similarly sized multirotors (Ref. 10), the crossover frequencies all fail to obtain the Froude scaled value which indicates the Froude scaled crossover doesn't represent a suitable design minimum for this vehicle class. Further, the crossover reduction between the lateral/longitudinal axes is pronounced with the lateral axis $\approx 5\%$ below Froude scaling in contrast to the longitudinal axis that is $\approx 50\%$ reduced and is a result of the higher pitch inertia. The V77 design produced excessively high crossover frequencies with reduced stability margins and degraded disturbance rejection capabilities, most notably in the form of high DRP. Comparing the DMO solution to the V77 design demonstrates significant improvements with increased stability margins in all axes, reduced crossover in the longitudinal/directional axes, and improved disturbance response qualities in all axes.

Disturbance response simulations were conducted with a 30(deg) initial condition offset to demonstrate the improved performance obtained by both the DMO and OPT design compared to V77. The lateral disturbance response for the simulation model depicted in Figure 6 demonstrates both CONDUIT[®] designs recover without oscillation. Note the DMO design has an initial recovery time approximately half that of the baseline OPT design as a result of the DRB minimum and crossover being pushed further into the Level 1 region. Figure 7 shows the longitudinal disturbance and exhibits improvements similar to the lateral axis. Lastly, Figure 8 demonstrates the oscillatory behavior of the V77 design in the directional axis in contrast to the well damped response of both the OPT and DMO designs.

Flight Test Validation

Flight test validation was performed for the inner-loop DMO design by conducting broken-loop frequency sweeps with the sweep injected before the mixer as indicated by δ_{latBL} in Figure 4. These sweeps allow the effective plant G and the feedback H to be independently validated in addition to

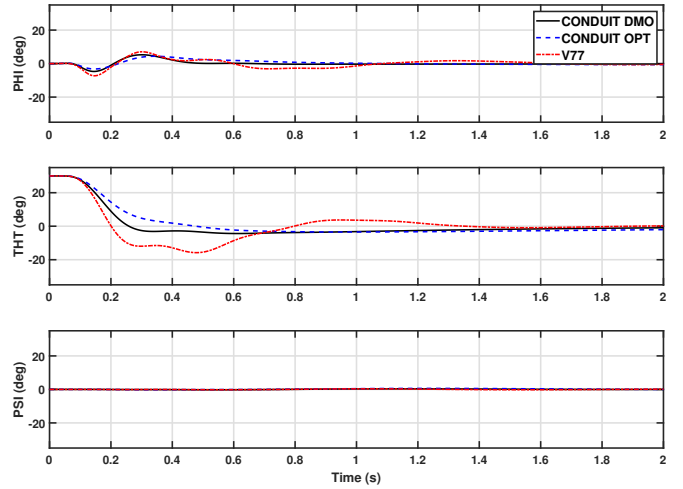


Figure 7. Disturbance Response Simulation for Pitch Initial Condition Offset

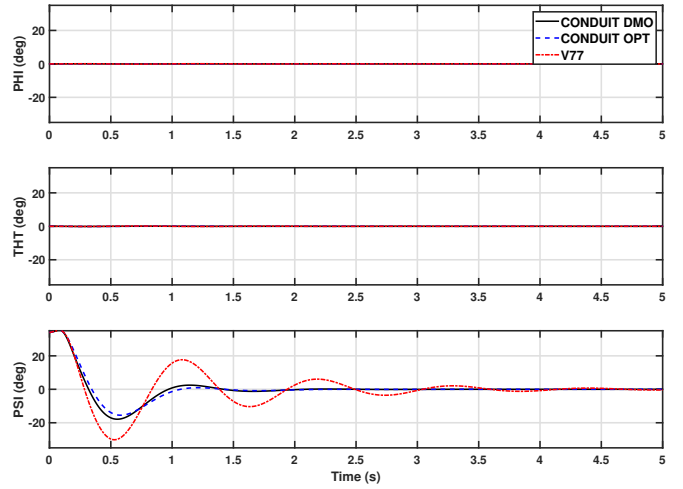


Figure 8. Disturbance Response Simulation for Yaw Initial Condition Offset

the overall broken loop response GH . Table 3 tabulates the key metrics from the broken-loop response for the lateral and longitudinal axis. These metrics were extracted from the broken-loop responses with Figure 9 depicting the lateral broken-loop response. Figure 10 depicts the closed-loop response ϕ/δ_{lat_s} , with the Maximum Unnoticeable Additional Dynamics (MUAD) boundary indicated by the shaded region (Ref. 13). The excellent agreement between flight test and the design model is a direct result of applying the black-box filter update.

OUTER-LOOP CONTROL DESIGN

The outer-loop controller provides Translational Rate Position Hold (TRPH) in the lateral, longitudinal, and heave axes. Figure 11 presents the architecture which consists of nested PI control loops and is mechanized in the local-level frame aligned with the vehicle heading as indicated by the R_ψ rotations following Ivler (Ref. 10). The input velocity command

Table 2. Inner-Loop Design Comparison

	V77 MANUAL	CONDUIT OPT	CONDUIT DMO	% Δ (DMO/OPT)	% Δ (DMO/V77)
<i>Lateral</i>					
GM (dB)	5.86	11.97	6.03	-49.62	2.99
PM (deg)	44.82	61.39	64.86	5.65	44.72
ω_{co} (rad/s)	7.19	6.33	10.64	67.99	47.99
DRB (rad/s)	4.07	4.10	5.73	39.68	40.88
DRP (dB)	3.73	3.07	5.00	62.81	34.21
<i>Longitudinal</i>					
GM (dB)	4.58	10.02	7.59	-24.20	65.92
PM (deg)	42.50	63.49	56.86	-10.44	33.78
ω_{co} (rad/s)	7.47	4.00	5.82	45.69	-22.10
DRB (rad/s)	3.86	2.40	3.37	40.44	-12.71
DRP (dB)	5.87	3.40	4.81	41.74	-18.01
<i>Directional</i>					
GM (dB)	6.33	8.80	7.33	-16.73	15.76
PM (deg)	40.18	42.55	48.59	14.21	20.92
ω_{co} (rad/s)	12.86	9.17	9.36	2.12	-27.22
DRB (rad/s)	3.48	3.21	3.79	17.96	8.98
DRP (dB)	9.98	5.00	5.00	0.0	-49.91

Table 3. Inner-Loop DMO Design v. Flight Test

	Design	Flight
<i>Lateral</i>		
GM (dB)	6.03	5.99
PM (deg)	64.86	64.90
ω_{co} (rad/s)	10.64	9.76
<i>Longitudinal</i>		
GM (dB)	7.59	7.48
PM (deg)	56.86	49.15
ω_{co} (rad/s)	5.82	5.51

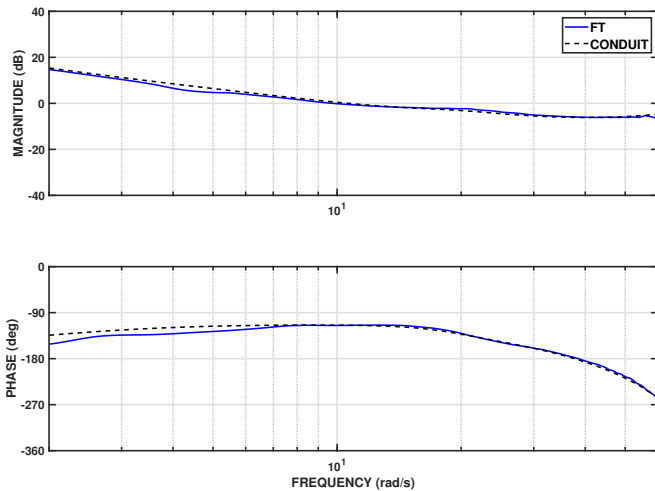


Figure 9. Lateral Inner-Loop Broken-Loop Response

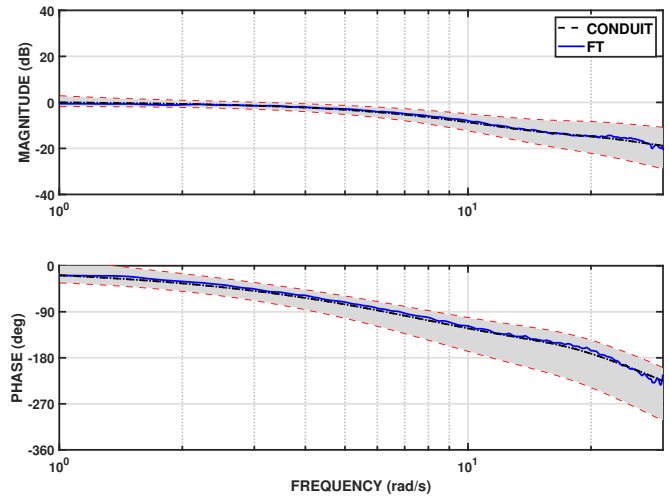


Figure 10. Lateral Inner-Loop Closed-Loop Response

is integrated to generate a reference position command used by the position loop to generate a velocity command contribution. The velocity loop produces an attitude command used by the inner-loop, except for the heave axis that generates a collective command. The PI architecture is the same for all loops with a lead-lag filter on the velocity controllers to shape the response as depicted in Figure 12 for the lateral velocity controller.

Optimization Using CONDUIT®

The outer-loop specifications are tabulated in Table 4. The stability margins and Nichols specifications are applied to the inner-loop broken at the actuator with outer-loops closed in addition to the outer velocity and position loops broken at

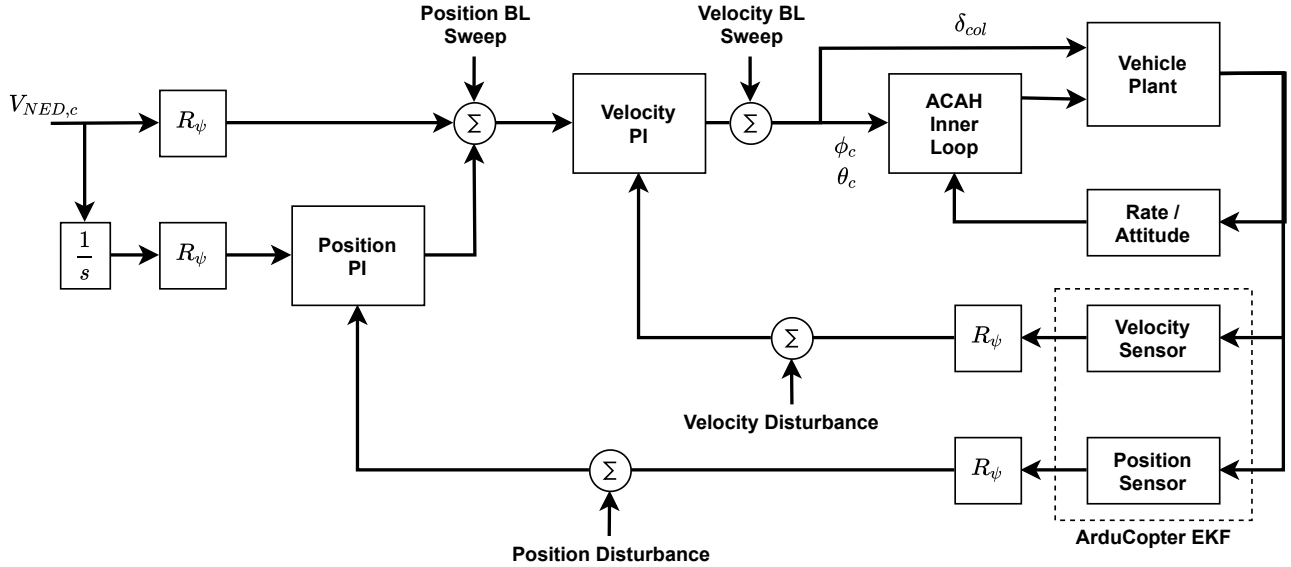


Figure 11. Translational Rate Position Hold Architecture

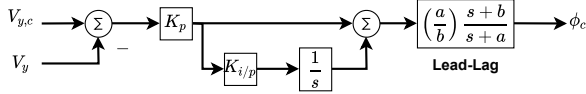


Figure 12. Lateral Velocity PI Architecture

Table 4. Outer-Loop Design Specifications

Specification	Constraint Type
Eigenvalues	Hard
Nichols	Hard
Stability Margins	Hard
Minimum Crossover	Soft
DRB	Soft
DRP	Soft
Heave Shipboard Response	Soft
Damping Ratio	Soft
Model Following	Soft
Open-Loop Onset	Soft
Maximum Crossover	Summed Objective
Actuator RMS	Summed Objective
CETI RMS	Check Only

their effective actuator as indicated by the broken-loop sweep injection points in Figure 11. The lateral and longitudinal velocity crossover frequencies were initially set to 1/5 of the corresponding inner-loop crossover frequency and the position loop crossover was similarly established. This ensures sufficient frequency separation while allowing subsequent design margin optimization to increase the crossover frequency and still satisfy the 1/5 – 1/3 frequency separation guideline of Reference 13. The crossover frequency for the heave velocity axis was established using the $\omega_{co} \geq (2-3)\omega_{unstable}$ guideline (Ref. 13) noting that the vehicle has an unstable heave mode at 1.24 (rad/s).

Froude scaling was applied to the heave shipboard response

and the heave velocity DRB. The Froude scaled heave position DRB is relatively low for the scale of this vehicle and was increased by a factor of three which relates the hover/low-speed heave response requirement to the shipboard landing requirement (Ref. 7). The lateral and longitudinal velocity/position DRB were also scaled; however, these responses are coupled to the inner-loop and as a result, require application of reduced Froude scaling. It is recommended to retain the relative ratio of the full-scale velocity DRB specification which is achieved by considering the limiting axis, in this case longitudinal, to define the reduction factor and then use the full-scale relative ratio to obtain the non-limiting axis boundary. This approach is similarly followed for the position loop.

The outer-loop is optimized with the inner-loop gains fixed except for the lateral and longitudinal command model frequencies which are left as free design parameters. Similar to the inner-loop, an initial *minimum* design is first optimized that satisfies all specifications to Level 1 boundaries. Design margin optimization is then conducted with design margin applied to the crossover and DRB specifications. Following the procedure of Reference 13 it is recommended that both the velocity and position loops are optimized simultaneously during the DMO process which ensures the velocity/position loops are balanced in terms of aggressiveness.

Table 5 tabulates the baseline optimized design compared to the final DMO solution for the longitudinal axis. The velocity and position crossover frequencies have been increased by approximately 30% and are both on the edge of the minimum frequency separation guideline. Both the velocity and position DRB have also been increased by $\approx 30\%$ which is reflected in an 18% reduction in the CETI RMS specification. However, the lateral and longitudinal controllers have an average 15% lower DRB than the Froude scaled specification which is significant as Froude scaling the full-scale specification is intended to represent the *minimum* acceptable design. This

Table 5. Outer-Loop Design Margin Optimization for Longitudinal Axis

	OPT	DMO	% Δ
<i>Longitudinal Velocity</i>			
GM (dB)	15.20	13.30	-12.52
PM (deg)	53.89	48.24	-10.48
ω_{co} (rad/s)	1.50	1.91	27.30
DRB (rad/s)	1.06	1.27	20.17
DRP (dB)	3.73	4.33	16.31
<i>Longitudinal Position</i>			
GM (dB)	12.89	11.38	-11.67
PM (deg)	70.92	70.58	-0.48
ω_{co} (rad/s)	0.51	0.66	29.4
DRB (rad/s)	0.38	0.50	31.6
DRP (dB)	3.00	3.26	8.70
CETI RMS (m)	0.61	0.56	-7.54

suggests that single main rotor UAVs may require different minimums than the more heavily researched multirotor vehicles which can attain full Froude scaling as demonstrated by References 9, 10.

Flight Test Validation

The outer-loop DMO design was validated in flight by conducting broken-loop and disturbance rejection sweeps. The location of the sweep inputs are depicted in Figure 11. Note the disturbance response sweeps are applied in the local lateral/longitudinal axes in order to isolate the controllers of interest. The lateral velocity and position broken-loop responses are presented in Figures 13 and 16 respectively. The velocity broken-loop response has quadratic cost of 21 and the position has a cost of 73 which demonstrates a single input correction addresses all the control loops. The lateral velocity closed-loop response is shown in Figure 14 and has excellent agreement with the design model that is well within the MUAD boundary. Figure 15 present the lateral velocity DRB which demonstrates excellent agreement between the design model and flight test. The key stability, crossover and disturbance response metrics for the lateral and longitudinal outer-loops are tabulated in Table 6 which demonstrate the design model accurately predicted the flight performance as a result of the broken-loop corrections used in the design process.

FLIGHT TEST MANEUVERS

The performance of the optimized controller was demonstrated in flight by conducting hover position-hold in windy conditions and dynamic maneuvers to include lateral/longitudinal reposition and pirouettes. The lateral reposition and pirouette maneuvers were Froude scaled to provide an appropriate measure of performance (Ref. 10). The longitudinal reposition maneuver utilized the same input command as the lateral reposition and is not representative of the ADS-33 depart-abort maneuver. Reference 10 introduced the tracking precision metric ϵ to quantify the vehicle's performance when evaluating MTEs. This metric is computed using

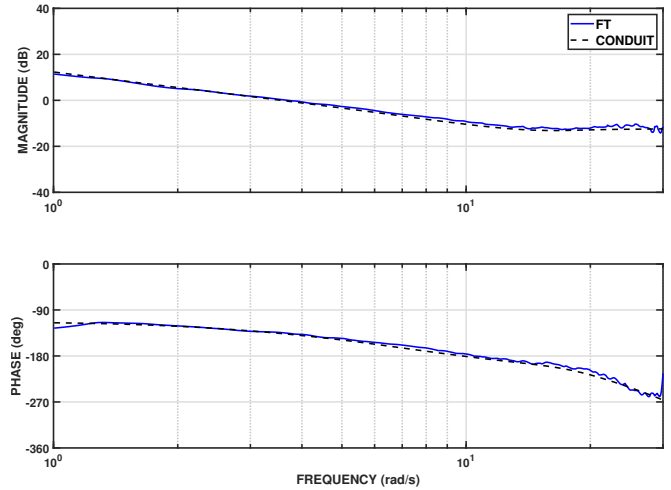


Figure 13. Lateral Velocity Control Broken-Loop Response

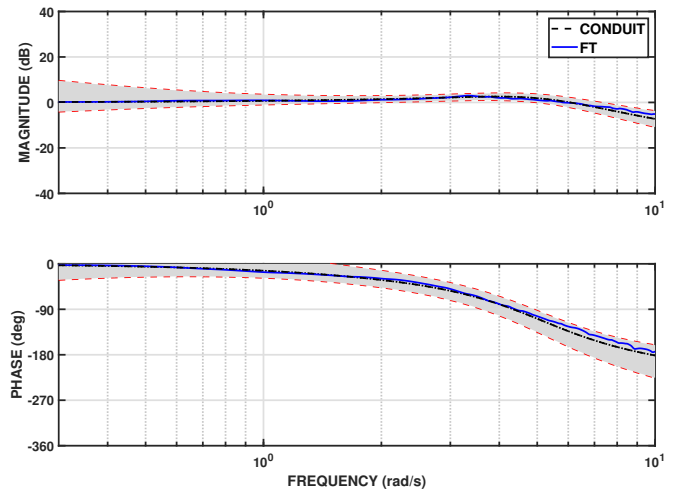


Figure 14. Lateral Velocity Closed-Loop Response

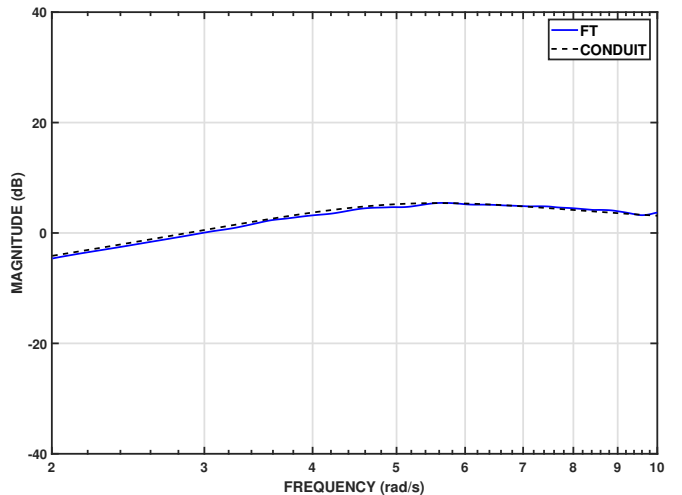


Figure 15. Lateral Velocity DRB

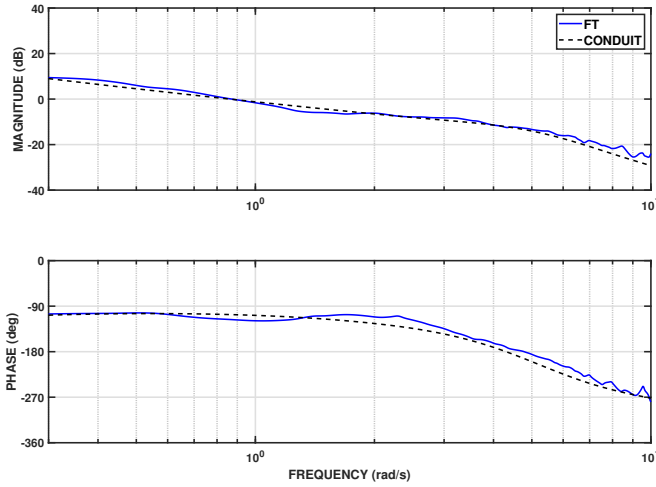


Figure 16. Lateral Position Control Broken-Loop Response

Equation 3 where $V_{max,cmd}$ is the maximum velocity command during the maneuver, L_{path} is the length of the maneuver, and V_{error} , P_{error} are the velocity and position error magnitudes calculated at each time step.

$$\varepsilon = w_V \frac{\text{rms}(V_{error})}{V_{max,cmd}} + w_P \frac{\text{rms}(P_{error})}{L_{path}} \quad (3)$$

The Froude scaled lateral repositioning maneuver consists of repositioning 6(m) in 4 seconds. This maneuver was commanded using a 3(m/s) impulse velocity command with a two second pulse-width in order to achieve the reposition in the desired time. Figure 17 depicts the Froude scaled lateral repositioning maneuver which exhibits minimal off-axis response. The maneuver was repeated multiple times and the mean tracking precision was computed to be $\varepsilon = 0.21$ which is well above the recommended adequate value of $\varepsilon = 0.15$ (Ref. 10). Note the undesirable tracking precision is an artifact of the impulse command used. It is recommended that a ramp velocity command be used following the work of Ivler (Ref. 10) to more appropriately align with the natural velocity response depicted in the velocity subplot of Figure 17 which would result in a satisfactory tracking precision metric.

Figure 18 depicts the longitudinal repositioning maneuver which used a command input identical to the lateral repositioning. This maneuver does not represent a Froude scaled MTE and is intended to demonstrate the minimal off-axis excitation of the vehicle during aggressive acceleration/deceleration in the longitudinal axis. Similar to the lateral maneuver, the tracking precision is undesirable with a computed value of $\varepsilon = 0.2635$ and is an artifact of the impulse command.

The Froude scaled pirouette maneuver has a radius of 1.5(m) with a translational velocity command of 1(m/s) and should be completed in 10 seconds. Unlike the lateral repositioning maneuver, the velocity command was passed through a critically damped second order filter to avoid an abrupt velocity command at the start of the maneuver. Figure 19 depicts the ma-

Table 6. Outer-Loop DMO Design v. Flight Test

	Design	Flight
<i>Lateral Velocity</i>		
GM (dB)	10.17	9.66
PM (deg)	43.96	44.47
ω_{co} (rad/s)	3.56	3.69
DRB (rad/s)	2.22	2.30
DRP (dB)	5.41	5.44
<i>Longitudinal Velocity</i>		
GM (dB)	13.30	13.84
PM (deg)	48.24	55.34
ω_{co} (rad/s)	1.91	1.92
DRB (rad/s)	1.27	1.29
DRP (dB)	4.33	4.09
<i>Lateral Position</i>		
GM (dB)	12.15	12.80
PM (deg)	73.34	63.41
ω_{co} (rad/s)	0.86	0.87
DRB (rad/s)	0.66	0.69
DRP (dB)	2.75	2.88
<i>Longitudinal Position</i>		
GM (dB)	11.38	13.32
PM (deg)	70.58	71.72
ω_{co} (rad/s)	0.66	0.64
DRB (rad/s)	0.50	0.55
DRP (dB)	3.26	3.03

neuver using the baseline optimized (OPT) outer-loop controller in orange and the DMO solution in blue. The arrows indicate the vehicle heading as it follows the pirouette trajectory where the directional axis is commanded with a constant yaw rate. The DMO design provides superior tracking with $\varepsilon = 0.1013$ and the baseline design has a tracking precision of $\varepsilon = 0.1506$. Note the change in tracking performance only reflects the longitudinal axis improvements tabulated in Table 5 as the lateral axis controller used was the same for both the baseline and DMO solution flown.

The hover position-hold maneuver was conducted on a relatively windy day with 3(m/s) winds and 3.6 – 4.5(m/s) gusts. Flights were conducted using both the empirically tuned ArduCopter position hold mode and the CONDUIT® DMO design with the tests conducted successively to ensure similar ambient conditions. Figure 20 depicts the hold performance of the two controllers where the vehicle was facing due West and the reference hold position command is the origin. The optimized design provides a significant improvement in performance with a lateral RMS of 0.1774(m), an 82% reduction, and a longitudinal RMS of 0.1946(m), an 84% reduction. The altitude performance had a modest improvement with a RMS of 0.0221(m), a 39% reduction. This demonstrates the substantial improvement in performance that can be obtained using model-based design.

CONCLUSIONS

This effort applied black-box filters to update the design model and used Froude scaled ADS-33 specifications with

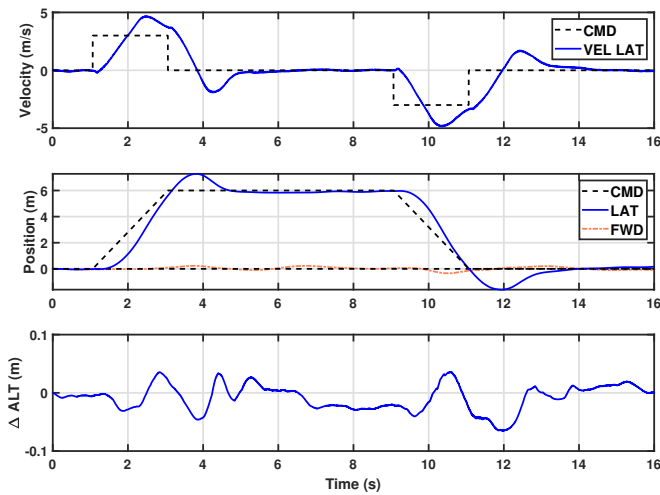


Figure 17. Lateral Reposition, DMO Outer-Loop

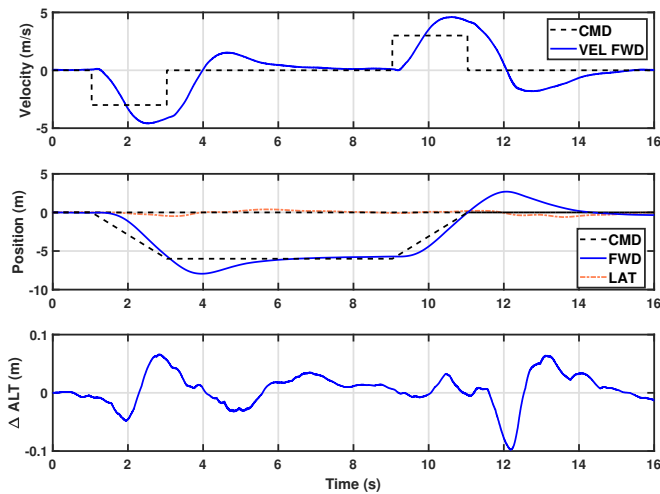


Figure 18. Longitudinal Reposition, DMO Outer-Loop

CONDUIT[®] to design an optimized inner- and outer-loop controller. Key elements of the development process were identification and application of black-box filters to update the model, Froude scaled design specifications with systematic optimization of the controllers, and validation and demonstration in flight using scaled MTEs. The results of this effort showed that:

1. Black-box input filters are an effective method for updating bare-airframe dynamics. Application of these corrections to the sub-scale flybarless helicopter resulted in excellent agreement between design and flight test.
2. Methodical control design using CONDUIT[®] enabled design of an optimized inner- and outer-loop controller that satisfied scaled ADS-33 requirements.
3. Design Margin Optimization allowed further performance to be obtained beyond the prescribed minimum design specifications. The improved performance was demonstrated by the adequate pirouette tracking of $\epsilon =$

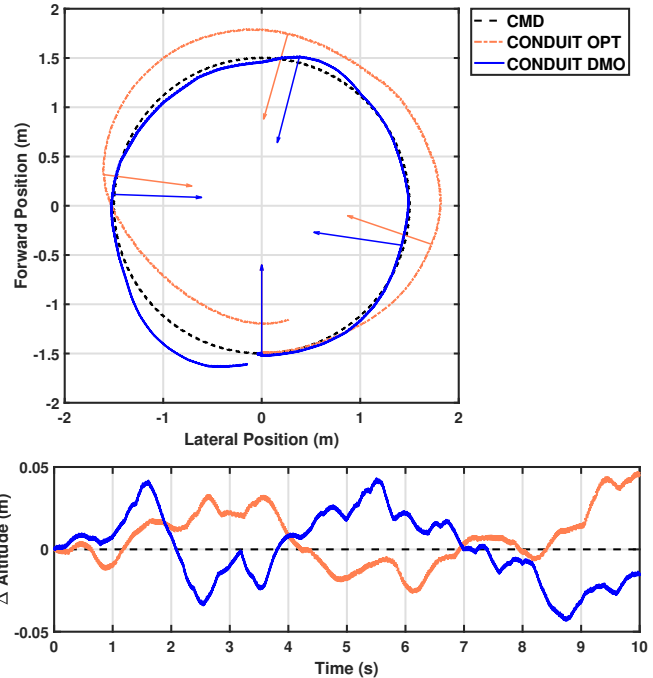


Figure 19. Pirouette Optimized v. DMO Outer-Loop

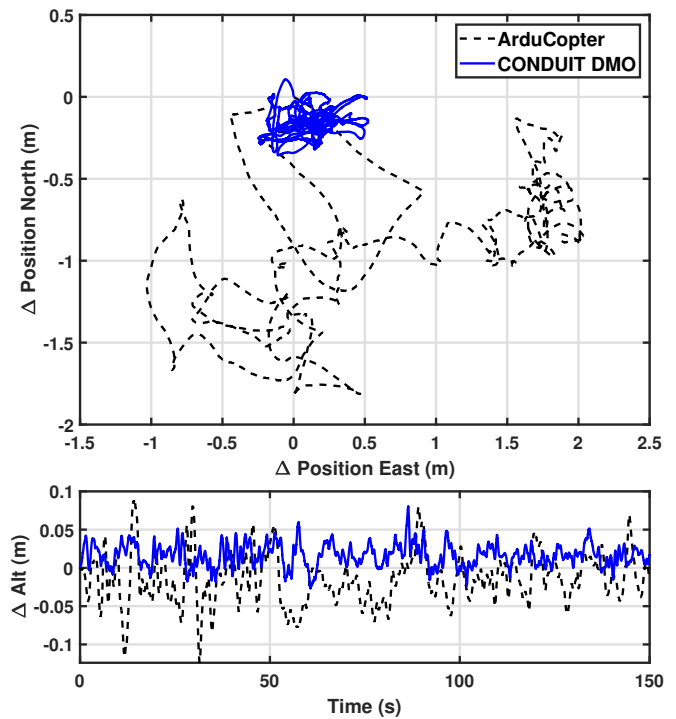


Figure 20. Hover Hold Optimized Control v. ArduCopter

- 0.1506 with the optimized design and desired tracking of $\varepsilon = 0.1013$ using the DMO design.
- Single main rotor UAS do not strictly adhere to Froude scaling specifications due to the rotor/fuselage coupling. Further research into minimum specifications for this class of vehicles is warranted.
 - Flight test maneuvers demonstrated satisfactory trajectory tracking performance. The optimized control design provided improved performance with an 82% reduction in lateral and 84% reduction in longitudinal RMS compared to the empirically tuned ArduCopter controller.

Author contact:

Jeffrey Walker jwalker@bihrl.com

Mark B. Tischler mrtischler@aol.com

REFERENCES

- FAA, "Certification for Advanced Operations Unmanned Aircraft Systems (UAS) Criteria for Special Classes," <https://www.faa.gov/uas/advanced-operations/certification/criteria-special-classes/>, 2022.
- "PX4," <https://px4.io/>.
- "ArduPilot," <https://www.ardupilot.org>.
- Tischler, M., and Remple, R. K., *Aircraft and Rotorcraft System Identification Engineering Methods with Flight Test Examples*, AIAA Education Series, AIAA, Reston, VA, second edition, November 2012.
- Tischler, M., White, M. D., D'Agosto, S., Cameron, N., Greiser, S., Gubbels, A., Guner, F., He, C., Horn, J., Hui, K., Jones, M., Juhasz, O., Lee, O., Lehmann, R., Miller, D., Myrand-Lapierre, V., Nadeau-Beaulieu, M., Nadell, S., Padfield, G., Pavel, M., Prasad, J., Ragazzi, A., Richard, S., Scepanovic, P., Seher-Weiß, S., Soong, J., Stroosma, O., Taghizad, A., Tobias, E., Xin, H., and Yavrucuk, I., "Rotorcraft Flight Simulation Model Fidelity Improvement and Assessment," STO-TR-AVT-296-UU, NATO, 2021.
- Greiser, S., Seher-Weiß, S., Scepanovic, P., Nadeau-Beaulieu, M., Myrand-Lapierre, V., and Gubbels, A., "Updating Rotorcraft Simulation Environments by Using "Black-Box" Input Filters," Proceedings of the 77th Annual Forum, Virtual, 2021.
- Anon, "Aeronautical Design Standard, Handling Qualities Requirements for Military Rotorcraft," ADS-33E-PRF, USAAMCOM, 2000.
- Berrios, M. G., Berger, T., Tischler, M., Juhasz, O., and Sanders, F. C., "Hover Flight Control Design for UAS Using Performance-based Disturbance Rejection Requirements," AHS 73rd Annual Forum, Fort Worth, Texas, 2017.
- Ivler, C., Goerzen, C., Wagster IV, J., Sanders, F., Cheung, K., and Tischler, M., "Control Design for Tracking of Scaled MTE Trajectories on an IRIS+ Quadcopter," American Helicopter Society 74th Annual Forum, Phoenix, Arizona, 2018.
- Ivler, C. M., Truong, K., Kerwin, D., Otomize, J., Parmer, D., Tischler, M., and Gowans, N., "Development and Flight Validation of Proposed Unmanned Aerial System Handling Qualities Requirements," Proceedings of the 76th Annual Forum, Virginia Beach, VA, 2020.
- Alvarenga, J., Vitzilaios, N., Rutherford, M., and Valavanis, K., "Scaled Control Performance Benchmarks and Maneuvers for Small-Scale Unmanned Helicopters," 54th IEEE Conference on Decision and Control (CDC), 2015.
- Walker, J., and Tischler, M., "Identification and Control Design of a Sub-Scale Flybarless Helicopter," Proceedings of the 77th Annual Forum, Virtual, 2021.
- Tischler, M., Cheung, K. K., and Soong, J. Y., *Practical Methods for Aircraft and Rotorcraft Flight Control Design: An Optimization-Based Approach*, AIAA Education Series, AIAA, Reston, VA, April 2017.
- Tischler, M. B., Lee, J. A., and Colbourne, J. D., "Comparison of Flight Control System Design Methods Using the CONDUIT Design Tool," *Journal of Guidance, Control, and Dynamics*, Vol. 25, (3), May 2002, pp. 482–493. DOI: 10.2514/2.4908
- Gong, A., Tischler, M. B., and Hess, R. A., "Deterministic Reconfiguration of Flight Control Systems for Multirotor UAV Package Delivery," Proceedings of the 77th Annual Forum, Virtual, 2021.
- Berger, T., Ivler, C., Berrios, M., Tischler, M., and Miller, D., "Disturbance Rejection Handling Qualities Criteria for Rotorcraft," AHS 72nd Annual Forum, West Palm Beach, Florida, 2016.
- Anon, "Aerospace - Flight Control Systems - Design, Installation and Test of Piloted Military Aircraft, General Specification For," AS94900, SAE, 2007.